An Optical Fiber-based SPR Sensor for Hepatocellular Carcinoma Detection

Renata Charlene Barbosa Xavier [*] **Jessica Neiva Alpino** [**]
Cleumar da Silva Moreira [***] **Rossana Moreno Santa Cruz** [****]

[*] *Department of Electrical Engineering, Federal Institute of Paraíba, PB, (e-mail: renatacharlene@gmail.com)*
[**] *Department of Electrical Engineering, Federal Institute of Paraíba, PB, (e-mail: jnalpino@gmail.com)*
[***] *Department of Electrical Engineering, Federal Institute of Paraíba, PB, (e-mail:cleumar.moreira@ifpb.edu.br)*
[****] *Department of Electrical Engineering, Federal Institute of Paraíba, PB, (e-mail: rossana.cruz@ifpb.edu.br)*

Abstract: An optical fiber-based surface plasmon resonance sensor for hepatocellular carcinoma diagnosis is presented here. Conventional, tip-based, and D-shaped configurations are used to construct the sensor. The sensing region length, the bimetallic layer, full width at half maximum (FWHM), figure of merit (FOM), sensitivity, and signal-to-noise ratio (SNR) have been used to analyze the sensor performance. The sensor setup uses three layers: a ZBLAN fluoride optical fiber core (optical substrate), a 40 nm-gold or 40 nm-silver films (plasmonic metal), and healthy and pathological samples (analyte). Moreover, a bimetallic layer has been also investigated, where the thicknesses ranged from 10 nm to 40 nm. Also, the sensing region varied from 5 mm to 60 mm. The results obtained for the sensitivity of the simulated sensors were: $3,903.4$ nm/RIU for gold, $3,821.5$ nm/RIU for silver, and $3,415.1$ nm/RIU for silver-gold layer.

Keywords: Surface plasmon resonance; optical fiber sensor; hepatocellular carcinoma; ZBLAN; performance.

1. INTRODUCTION

Hepatocellular carcinoma (HCC) is the seventh most common cancer and the third leading cause of cancer-related deaths worldwide. Liver cancer is almost always preceded by chronic liver damage, most commonly caused by the hepatitis B virus (Gravitz, 2014). Primary liver cancer comprises hepatocellular carcinoma (HCC) and intrahepatic cholangiocarcinoma (ICC), which are distinct in morphology, metastatic capacity and response to cancer therapy (Seehawer et al., 2018). The liver is a common site of metastases, particularly colorectal carcinoma, while it is estimated that up to two-thirds of patients with colorectal liver metastases die from their disease (Giannios et al., 2016). In this way, discover a disease early can reduce the chance of mortality and treat the individual in a more controlled way.

SPR is a very sensitive technique used for determining small refractive index changes at the metal-dielectric interfaces. In SPR sensors, light can be coupled through diffraction on periodic metallic gratings (Perino et al. (2014)), prisms (Oliveira et al. (2013)), or optical fibers (Shibayama et al. (2016)).

Optical fibers based on fluoride (FOFs) can be exploited in SPR-based chemical- and biosensing. Fluoride glasses are the only materials that continuously transmit light from the ultraviolet to the infrared region, which is an advantage for the manufacture of high quality optical fibers (Saad, 2009). Such materials are increasingly examined for applications in the following areas: medicine, spectroscopy and detection, amplifiers and fiber lasers, data transmission (ultra-long, submarine), and advanced sensors (Cozmuta et al., 2020).

The composition of the best known standard fluoride glass is based on zirconium fluoride, commonly called the fluorozirconate family or ZBLAN, as it contains in its formation 53% zirconium fluoride - ZrF_4, 20% barium fluoride - BaF_2, 4% lanthanum fluoride - LaF_3, 3% aluminum fluoride - AlF_3, and 20% aluminum fluoride sodium - NaF. They are more stable fluoride-based glasses and very adequate for manufacturing of FOFs Jin et al. (2011). ZBLAN optical fibers have low optical loss coefficients and a wide transmission window, which can vary from 300 nm to 4500 nm.

Here, we perform a theoretical investigation considering a ZBLAN fluoride-based optical fiber for SPR sensing applications. Gold (Au), Silver (Ag), and a bimetallic layer (composed by Au and Ag) are used as the plasmonic materials. Samples are from an experimental data for healthy and pathological liver tissues. Sensitivity, full width at half maximum (FWHM), figure of merit (FOM), and signal-to-noise ratio (SNR), are calculated to investigate the sensor performance. These parameters are function of the sensing region length for conventional, tip-based, and D-shaped biochips.

2. THEORETICAL METHOD

The Fresnel-Abelès multilayer model is used to calculate the intensity of the light reflected by a p-polarized incident beam (Oliveira et al. (2013)). The scheme of the multilayer system is shown in Fig. 1, where n_k is the refractive index and d_k is the thickness of layer k. The model assumes that all layers are non-magnetic, uniform and isotropic. Because of the partial transmission on the z-axis in the sensing region, part of the power incident on the fiber core (first layer) fades through other layers by absorption.

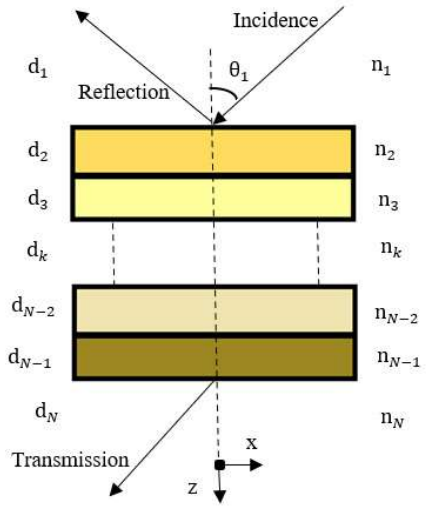

Figura 1. Schematic of the N-layer method.

The matrix model uses Maxwell's equations that are in accordance with the boundary conditions between two adjacent layers in order to calculate the propagation of radiation through the multilayer system. In this way, the components of the electric and magnetic field vectors in the initial and final limits are related by Moayyed et al. (2014):

$$\begin{bmatrix} U_1 \\ V_1 \end{bmatrix} = M \begin{bmatrix} U_{N-1} \\ V_{N-1} \end{bmatrix}, \tag{1}$$

where, U_1 and V_1 are respectively, the tangential components of the electrical system and magnetic fields, at the limit of the first layer.The field components in the contour of the last layer are represented by U_{N-1} and V_{N-1}.The characteristic matrix of the complete system is presented by M, found through the individual matrices of each interface or layer of the system, given by Tabassum and Gupta (2016):

$$M = \prod_{k=2}^{N-1} M_k = \begin{bmatrix} m_{11} & m_{12} \\ m_{21} & m_{22} \end{bmatrix}, \tag{2}$$

the resultant of the matrix, M_k represents the propagation from the k layer to the $k+1$ layer. The resultant of the matrix, or the individual transference matrix can be defined as Yuan et al. (2011):

$$M_k = \begin{bmatrix} \cos\beta_k & -i\sin\beta_k/q_k \\ -iq_k\sin\beta_k & \cos\beta_k \end{bmatrix}, \tag{3}$$

where, q_k represents the optical admittance as a function of the polarization, since the surface plasmons are excited by a p-polarized wave, given by $(n_k^2 - n_1^2\sin^2\theta_1)^{1/2}/n_k^2$, and β_k is the phase factor of the k-layer, given by $(2\pi d_k/\lambda)(n_k^2 - n_1^2\sin^2\theta_1)^{1/2}$. Fresnel equations are used to calculate the reflection coefficient for a p-polarized incident wave, defined by:

$$r_p = \frac{(m_{11} + m_{12}q_N)q_1 - (m_{21} + m_{22}q_N)}{(m_{11} + m_{12}q_N)q_1 + (m_{21} + m_{22}q_N)}. \tag{4}$$

The reflectance (R_p) of a multilayer system for a p-polarized light is obtained as:

$$R_p = |r_p|^2. \tag{5}$$

Inside the optical fiber, the light rays propagates within an angular range that vary between the values of the critical angle, ($\theta_c = \arcsin(n_2/n_1)$) to $\theta = \pi/2$, where n_2 and n_1 are the refractive indexes of fiber cladding and fiber core.The normalized transmitted power through the sensing region of the biochip is described as Mishra et al. (2016):

$$P_{trans} = \frac{\int_{\theta_c}^{\frac{\pi}{2}} R_p^{N_{ref}(\theta)} \frac{n_1^2\sin\theta\cos\theta}{(1-n_1^2\cos^2\theta)^2} d\theta}{\int_{\theta_c}^{\frac{\pi}{2}} \frac{n_1^2\sin\theta\cos\theta}{(1-n_1^2\cos^2\theta)^2} d\theta}, \tag{6}$$

where, $N_{ref}(\theta)$ is the number of reflections of the light beam within the fiber. With this parameter, it can be said that the greater the length of the sensor or fiber region. For a conventional biochip shape, with the sensing region in a central portion of the optical fiber, the total number of internal reflection is calculated as Yuan et al. (2011):

$$N_{ref}(\theta) = \frac{L}{D\tan\theta}, \tag{7}$$

in which, D is the fiber core diameter and L is the length of the sensing region. For the biochip with sensing region at the optical fiber tip, the total number of internal reflections is defined as Wei et al. (2017):

$$N_{ref}(\theta) = \frac{2L}{D\tan\theta}. \tag{8}$$

A D-shaped biochip comprises a side-polished optical fiber in which the cladding and part of the core are removed. In this case, the total number of internal reflections is described by Sequeira et al. (2016):

$$N_{ref}(\theta) = \frac{L\tan\theta}{2(r+h)}, \tag{9}$$

where, r is the fiber radius and h is the polishing depth, that is, the distance from the core center to the polished surface plane.

2.1 Performance parameters of the optical fiber-based SPR sensor

The performance analysis of the optical fiber-based SPR sensors can be performed by calculating four different parameters: (i) sensitivity, (ii) full width at half maximum (FWHM), (iii) figure of merit (FOM), and (iv) signal-to-noise ratio (SNR). For a sensor working in the wavelength interrogation mode (WIM), the sensitivity refers to the resonant wavelength variation, $\delta\lambda_{res}$ with respect to a variation, δn_s, in the refractive index of the surrounding medium, n_s. Thus, the refractometric sensitivity for an optical fiber-based SPR sensor is given as Mishra et al. (2016):

$$S_n = \frac{\delta\lambda_{res}}{\delta n_s}. \tag{10}$$

FOM relates two parameters (sensitivity and FWHM) in a single performance parameter, and it provides information about the resonance wavelength shift and the sensor accuracy. For calculate the overall sensor parameter, FOM is defined by Lin et al. (2012):

$$FOM = \frac{S_n}{FWHM}. \quad (11)$$

SNR provides information about how precise a SPR sensor is. The detection accuracy of the resonant wavelength (and hence of the surrounding medium RI) is an important performance parameter. As SNR is inversely proportional to the SPR curve width at a specific level of transmitted power, the narrower the width, the higher the accuracy. SNR can be expressed as Dwivedi et al. (2008):

$$SNR = \frac{\delta\lambda_{res}}{FWHM}. \quad (12)$$

In this analysis, we considered the SPR curve width being equal to the FWHM for all the calculated parameters.

3. SENSOR DESCRIPTION

Theoretical analysis considered the following fiber dimensions: a ZBLAN core (usually composed of 53 % zirconium fluoride - ZrF_4, 20 % barium fluoride - BaF_2, 4 % lanthanum fluoride - LaF_3, 3 % aluminum fluoride - AlF_3 and 20 % sodium fluoride - NaF) with core diameter of 400 μm, and ultraviolet curable acrylate cladding of 600 μm (Gan (1995)).

The used metallic substrates were a thin gold film and a thin silver film, being each one with a thickness of 40 nm, and the length of the sensing region varied from L = 5 mm to L = 60 mm. In addition, a bimetallic layer was also used, with layer thickness ranging from 10 nm to 40 nm.

Regarding the biochip shape, we evaluated three different structures: (i) conventional, with the sensing region in an uncladded central portion of the fiber; (ii) sensing region in one of the optical fiber tips; (iii) D-shaped, with the sensing region in a side-polished portion of the optical fiber. At the conventional and D-shaped biochips, light from a polychromatic source is launched into one end of the fiber, and the output transmission spectrum is recorded on the other end. On the other hand, at the tip biochip, light is launched and recorded on one end of the optical fiber. Fig. 2 depicts these structures.

3.1 Human liver tissue refractive index

A study by Giannios et al. (2016) verified the refractive index for five groups of liver tissue, including healthy tissues with hepatocellular carcinoma and metastasis. Identifying hepatic IR is critical to expanding diagnostic options with optical devices. The mean real refractive indices were measured and fitted to the Cauchy equation with three standard terms, where the value of R^2 was greater than 0.98, varying the spectrum from 450 nm to 1551 nm. According to Giannios et al. (2016), Equations (13) and (14) serve to calculate the refractive index, as a function of the wavelength, and are described below:

$$n_{healthy}(\lambda) = 1.3591 + \frac{0.00827}{(\lambda^2)} + \frac{(-0.000576)}{(\lambda^4)}, \; and \quad (13)$$

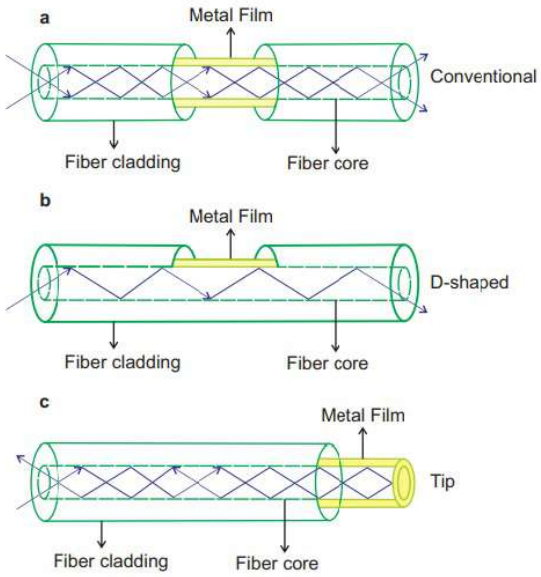

Figura 2. Schematic diagram of the investigated biochips: (a) Conventional, (b) D-shaped sensing regions, and (c) Tip.

$$n_{pathological}(\lambda) = 1.34348 + \frac{0.00998}{(\lambda^2)} + \frac{(-0.000793)}{(\lambda^4)} \quad (14)$$

In both equations, the wavelengths must be considered in nanometers to perform the Refractive Index (RI) calculations. This study Giannios et al. (2016) revealed that the actual and imaginary refraction indices of cancer tissues are superior, with regard to the normal state of the liver. The complex RI of ZBLAN, Gold (Au) and Silver (Ag) were obtained interpolating the experimental data found in Gan (1995); McPeak et al. (2015).

4. RESULTS AND DISCUSSION

The proposed analysis has been carried out for a wavelength range between 400 nm and 1,200 nm. This wavelength range coincides with the wavelengths used by Giannios et al. (2016) in their measurement experiments.

4.1 Effect of the sensing region length

To compare the effects of the sensing region length on the performance parameters of the different biochip structures, we calculated the previously mentioned parameters for the sensing region length from $L = 5.0$ mm to $L = 60.0$ mm.

Figure 3 shows that FWHM increases for the three structures of the biochip in accordance of the increase of the sensing region length. The conventional one presented the best result of FWHM (91.06 nm for gold and 52.81 nm for silver).

Figure 4 exhibits the values of FOM, where the maximum FOM value for a conventional setup is 42.87 RIU^{-1} for gold and 72.36 RIU^{-1} for silver. These results are quite similar for a tip and D-shaped setups when silver is the plasmonic metal. A similar behavior is observed when SNR is calculated as can be seen in Fig. 5. The maximum values is quite similar for a silver-based configuration.

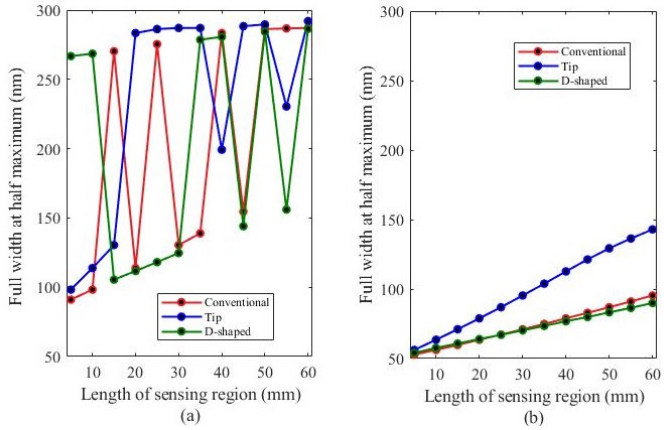

Figura 3. Variation of FWHM as a function of the sensing region length for the three biochip structures: (a) gold and (b) silver.

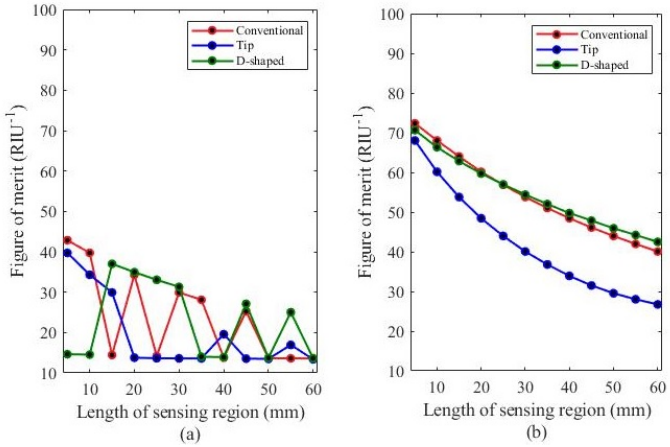

Figura 4. Variation of FOM as a function of the sensing region length for the three biochip structures: (a) gold and (b) silver.

The sensitivity reached a value of $3,903.4$ nm/RIU (gold) and 3821.5 nm/RIU (silver) for the proposed sensor with conventional configuration. We analyzed the response of the best structure (conventional at $L = 5.00$ mm) for the three healthy and pathological liver tissue samples measured by Giannios et al. (2016).

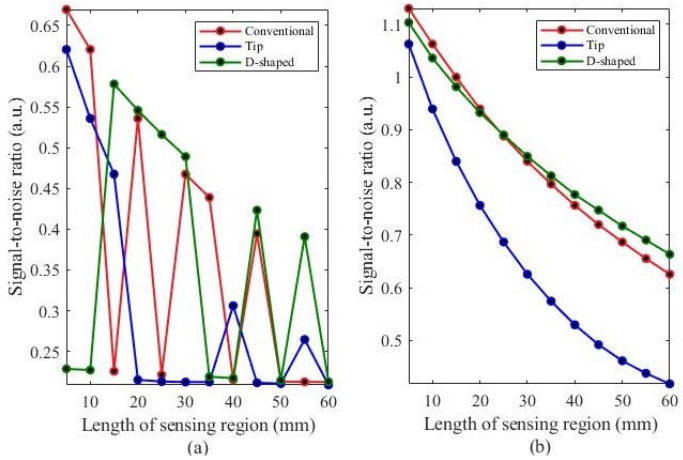

Figura 5. Variation of SNR as a function of the sensing region length for the three biochip structures: (a) gold and (b) silver.

4.2 Effect of the bimetallic coating

The metallic film of silver is more conductive than gold and has excellent optical properties, however silver can corrode and tarnish in wet environments (Sasaki et al., 2013). Thus, as the organs and specifically, the liver tissue presents in its formation, proteins, water and blood, it is necessary that there is a protection to avoid the wear of the metallic films and any other type of interference in the results. For that, we investigated a way to protect the metallic film of silver through a bimetallic layer.

For this analysis, we have been studied four different combinations for the silver and gold film thickness they are: (i) 40 nm Ag + 10 nm Au; (ii) 30 nm Ag + 20 nm Au; (iii) 20 nm Ag + 30 nm Au; and (iv) 10 nm Ag + 40 nm Au. The silver-gold ratio corresponds to the thickness relation of silver and gold films.

Fig 6 shows the variation of FWHM with the silver-gold ratio of the bimetallic coating, biochip with a 40nm-thick gold film has a value of 36.33 nm. Comparing the FWHM values of silver and gold with bimetallic, we observed that bimetallic layer has better results. Still in Fig 6 it is possible to see the inset exhibits the normalized transmitted power for the four bimetallic coating configurations: (i) 40 nm Ag + 10 nm Au - red line; (ii) 30 nm Ag + 20 nm Au - blue line; (iii) 20 nm Ag + 30 nm Au - green line; and (iv) 10 nm Ag + 40 nm Au - black line.

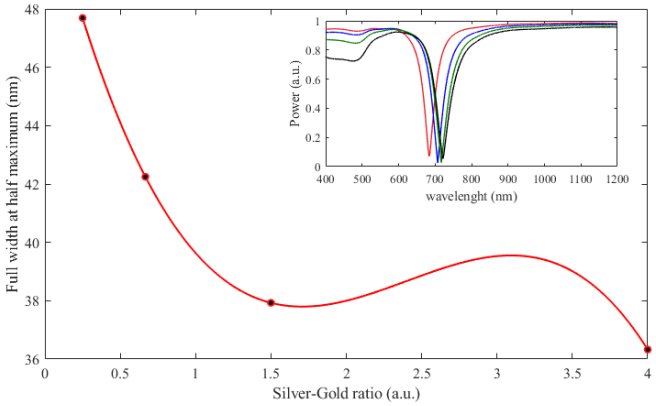

Figura 6. Variation of full width at half maximum with the silver-gold ratio.

Fig. 7 illustrates FOM and SNR variation of the bimetallic layer. FOM reaches the maximum value (92.51 RIU^{-1} for the bimetallic coating composed of 40 nm silver and 10 nm gold (silver-gold ratio equal to 4). FOM tends to decrease with the reduction of silver film thickness for the bimetallic configurations. In relation to the SNR, we observed that it decreases for the lowest values of the silver-gold ratio because of normalized transmitted power spectrum amplification. The deposition of the gold thin film also increases the SNR values, with a peak of 1.44.

Fig. 8 depicts the normalized transmitted power spectrum for the healthy and pathological liver. Three liver tissue samples were considered of each one. Comparing to the conventional structure with a gold and silver film, the structure with a bimetallic coating provides a deeper dip in the resonance wavelength.

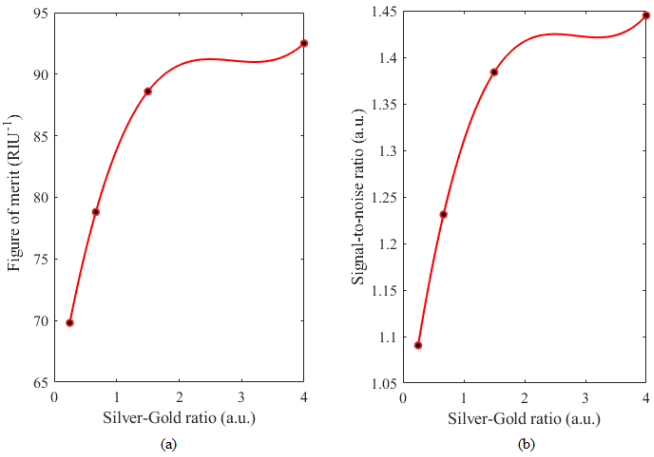

Figura 7. Variation (a) FOM and (b) SNR, with the silver-gold ratio.

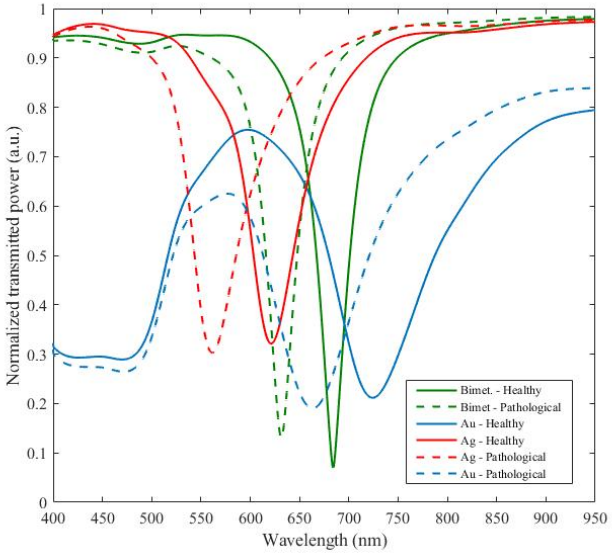

Figura 8. Normalized transmitted power for the healthy and pathological liver samples considering a conventional biochip.

Still in Fig. 8 we also identify narrowest curves and a blueshift of resonant wavelength for the structure with bimetallic coatings. The use of bimetallic coatings reduced the standard deviation when considered to the conventional structure with a silver film and gold. For the three samples of each analyzed tissues, the wavelength of resonance for healthy tissues does not coincide with the resonance wavelength for pathological tissues.

The addition of gold overlay on the silver film decreases the sensitivity reaching to 3415.1 nm/RIU. To calculate the sensitivity, a refractive index difference equal to the difference between the healthy and pathological liver tissue RI was assumed.

To better visualize the comparison of the results obtained in the study, the values of the performance parameters for a biochip (conventional structure, thin films of silver, gold and bimetallic layer) are listed in Table 1.

Tabela 1. Theoretical performance of the proposed SPR sensors.

Structure	S (nm/RIU)	FWHM (nm)	FOM (RIU^{-1})	SNR (a.u.)
Ag	3821.5	52.81	78.36	1.13
Au	3903.4	91.06	42.87	0.66
Ag+Au	3415.1	36.33	92.51	1.44

5. CONCLUSION

Here, we have proposed and theoretically investigated three configurations of ZBLAN optical fiber-based SPR sensors for hepatocellular carcinoma detection. Firstly, we have investigated the effects of thin metal films, gold and silver. Regarding the sensing region length, the smaller the sensing region, the higher the FOM and SNR parameters. In addition, we investigated the influence of a metallic layer to protect the biochip. The sensitivity reached a value of 3903.4 nm/RIU for gold, 3821.5 nm/RIU for silver, and 3415.1 nm/RIU for bimetallic layer, as plasmonic materials. In this way, such a fluoride optical fiber-based SPR sensor can be considered as an efficient, label-free, and accurate device to be used for hepatocellular carcinoma detection.

REFERÊNCIAS

Cozmuta, I., Cozic, S., Poulain, M., Poulain, S., and Martini, J.R.L. (2020). Breaking the silica ceiling: Zblan-based opportunities for photonics applications. 11276, 133 – 147. doi:10.1117/12.2542350.

Dwivedi, Y.S., Sharma, A.K., and Gupta, B. (2008). Influence of design parameters on the performance of a surface plasmon sensor based fiber optic sensor. *Plasmonics*, 3(2-3), 79–86.

Gan, F. (1995). Optical properties of fluoride glasses: a review. *Journal of Non-Crystalline Solids*, 184(2-3), 9–20.

Giannios, P., Koutsoumpos, S., Toutouzas, K.G., Matiatou, M., Zografos, G.C., and Moutzouris, K. (2016). Visible to near-infrared refractive properties of freshly-excised human-liver tissues: marking hepatic malignancies. *Scientific Reports*, 6, 1–10. doi:10.1038/srep27910.

Gravitz, L. (2014). Liver cancer. *Nature*, 516. doi:https://doi.org/10.1038/516S1a.

Jin, A., Wang, Z., Hou, J., Zhang, B., and Jiang, Z. (2011). Experimental measurement and numerical calculation of dispersion of zblan fiber. *International Coriference on Electronics and Optoelectronics*, 25, 181–184.

Lin, J.T., Cheng, D.C., Jiang, M., Chiang, Y.S., and Liu, H.W. (2012). Analysis of scaling law and figure of merit of fiber-based biosensor. *Journal of Nanomaterials*, 2012, 3.

McPeak, K.M., Jayanti, S.V., Kress, S.J.P., Meyer, S., Iotti, S., Rossinelli, A., and Norris, D.J. (2015). Plasmonic films can easily be better: Rules and recipes. *ACS Photonics*, 2(3). doi:10.1021/ph5004237.

Mishra, A.K., Mishra, S.K., and Verma, R.K. (2016). Graphene and beyond graphene mos2: a new window in surface-plasmon-resonance-based fiber optic sensing. *The Journal of Physical Chemistry C*, 120(5), 2893–2900.

Moayyed, H., Leite, I.T., Coelho, L., Santos, J.L., and Viegas, D. (2014). Analysis of phase interrogated spr fiber optic sensors with bimetallic layers. *IEEE Sensors Journal*, 14(10), 3662–3668.

Oliveira, L.C., da Silva Moreira, C., Thirstrup, C., Melcher, E.U.K., Lima, A.M.N., and Neff, H. (2013). A surface plasmon resonance biochip that operates both in the angular and wavelength interrogation modes. *IEEE Transactions on Instrumentation and Measurement*, 62(5), 1223–1232.

Perino, M., Pasqualotto, E., Scaramuzza, M., De Toni, A., and Paccagnella, A. (2014). Characterization of grating coupled surface plasmon polaritons using diffracted rays transmittance. *Plasmonics*, 9(5), 1103–1111.

Saad, M. (2009). Fluoride glass fiber: State of the art. *Proc SPIE*, 7316, 7160–7171. doi:10.1117/12.824112.

Sasaki, T., Kawamura, M., Abe, Y., and Kim, K. (2013). Suppression of property changes in ag thin films by introducing organic monolayers. *Vacuum*, 121.

Seehawer, M., Heinzmann, F., and et al., L.D. (2018). Necroptosis microenvironment directs lineage commitment in liver cancer. *Nature*, 562, 69–75. doi:https://doi.org/10.1038/s41586-018-0519-y.

Sequeira, F., Duarte, D., Bilro, L., Rudnitskaya, A., Pesavento, M., Zeni, L., and Cennamo, N. (2016). Refractive index sensing with d-shaped plastic optical fibers for chemical and biochemical applications. *Sensors*, 16(12), 2119.

Shibayama, J., Shimizu, K., Yamauchi, J., and Nakano, H. (2016). Surface plasmon resonance waveguide sensor in the terahertz regime. *Journal of Lightwave Technology*, 34(10), 2518–2525.

Tabassum, R. and Gupta, B.D. (2016). Spr based fiber-optic sensor with enhanced electric field intensity and figure of merit using different single and bimetallic configurations. *Optics Communications*, 367, 23–34.

Wei, W., Nong, J., Tang, L., Wang, N., Chuang, C.J., and Huang, Y. (2017). Graphene-mos 2 hybrid structure enhanced fiber optic surface plasmon resonance sensor. *Plasmonics*, 12(4), 1205–1212.

Yuan, Y., Ding, L., and Guo, Z. (2011). Numerical investigation for spr-based optical fiber sensor. *Sensors and Actuators B: Chemical*, 157(1), 240–245.